

Bipolar Spin Switch

Mark Johnson

A thin ferromagnetic film can be used to polarize the spin axes of the electrons carrying an electric current in a manner loosely analogous with a light polarizer. When such a film is fabricated on a gold film, a nonequilibrium population of spin-polarized electrons is built up in the gold causing a "spin bottleneck" effect. The addition of a second ferromagnetic film results in a device whose output voltage depends on the orientation of the spins.

An electronic switching device is introduced that, in contrast to solid-state devices, which are made from semiconductors, has been fabricated with only metals. Whereas the physical principles of semiconductor devices can be understood within a classical picture, this device relies on the spins of electrons and thus depends implicitly on quantum mechanics. Although the performance of semiconductor devices suffers with miniaturization, the gain of this device is inversely proportional to its size, so its operation characteristics improve as its size decreases. The device may have many uses, including direct application in magnetic information-storage technology.

The device is composed of a paramagnetic metal film P sandwiched between two ferromagnetic films F1 and F2 (Fig. 1A). Each ferromagnetic film is a single domain, and the axis of magnetization of each film, \hat{M}_1 and \hat{M}_2 , lies in the plane of the film. For simplicity, we consider the case in which \hat{M}_1 points down and \hat{M}_2 points either down or up. A battery is connected with one terminal to F1 and the other to the bottom of P. When the switch is closed, a current flows through F1 into P and is drained from P back to the battery. A third wire is attached to F2 and leads to a gedanken voltmeter, which can read the voltage V_{F2} of F2 with a single input and does not need a ground.

The details of the current transport and of the effect of current transport on V_{F2} can be understood with the use of a microscopic model and density-of-state diagrams (Fig. 1C). For the sake of simplicity, this model neglects the resistance of the films and of the interface between the films (1) and assumes there is no spin scattering at the interface itself. The diagrams have been drawn out of proportion to demonstrate the nonequilibrium effects. In reality, typical Fermi energies, E_F , are 5 to 10 V, the nonequilibrium effects, $E_{F,F2} - E_{F,0}$, are less than a millivolt, and thermal smearing (neglected in the figure) is of order 10 mV. The ferromagnets are depicted in a band model in which the majority-spin subband (that of downspins and that which deter-

mines the direction of \hat{M}_i) lies entirely below the Fermi level. This would be appropriate, though oversimplified, for the 3d band or a hybridized *sd* band of transition-metal ferromagnets, like Ni, Fe, Co, or an alloy, such as permalloy Ni_xFe_{1-x} . The paramagnet is represented with a free-electron model. With the switch open (Fig. 1C, faint diagrams), the Fermi levels of the contiguous metals align with value $E_{F,0}$.

When the switch is closed, an electric current, I_e , is driven from F1 to P. However, current transport involves only electrons of energy within a thermal range $E_F \pm k_B T$, where k_B is Boltzmann's constant and T is temperature. Because the downspin subband is well below E_F , only the upspin subband is available to carry the current. Thus, the electric current is also a current of magnetic dipoles; it is a spin-polarized electric current, and associated with the electric current is a current of magnetization (2, 3) $I_M = \eta_1 \beta I_e / e$, where β , the Bohr magneton, is the magnetic moment of each electron and e is the electron charge. Here,

η is a phenomenological parameter (3), $\eta = (J_\uparrow - J_\downarrow) / (J_\uparrow + J_\downarrow)$, where $J_{\uparrow,\downarrow}$ are the current densities of each spin subband, which describes the efficiency of spin transport. In the simplified model of Fig. 1C, $\eta = 1$, but more generally (3) the magnitude of η is diminished by current contributions from the other spin subband (if it does not lie entirely below E_F), and $|\eta| \leq 1$. Conceptually, F1 acts as a spin polarizer in a manner loosely analogous to a polarizing film for light but with the important difference that conduction electrons move diffusively, in contrast to photons.

I chose the thickness d of P to be less than a spin depth δ_s , the characteristic length over which an electronic spin can diffuse before undergoing a scattering event that randomizes the orientation of its spin. In the vicinity of F2, in a steady-state process, polarized spins are constantly being added to P at a rate I_M , and the polarization is being lost because of random scattering at a rate $1/T_2$, where T_2 is the spin relaxation time (4). As a result, a nonequilibrium magnetization builds up in P, $\bar{M} = I_M T_2 / Ad$, where A is the area of contact of F1 and Ad is the volume that the spins occupy in P. The net increase in occupation of the upspin subband is offset by a decrease in occupation of the downspin subband (Fig. 1C) so that charge neutrality is preserved. In Fig. 1A, the nonequilibrium spin magnetization is represented by the dotted cloud in P, and one can think of the combination of the electric current with the "spin polarizer" F1 as a "spin pump" that "pumps up" a nonequilibrium population of spins in P.

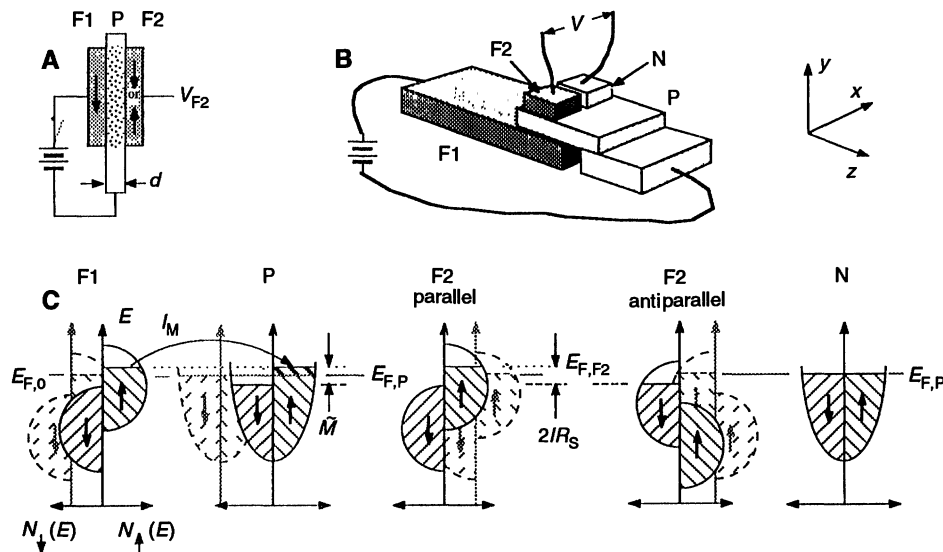


Fig. 1. (A) Pedagogical model of three-terminal device in cross section. Arrows in the ferromagnetic films F1 and F2, which sandwich the paramagnetic film P, refer to magnetization orientation as determined by majority-spin subband. (B) Geometry of a spin-switch device. N, nonmagnetic metal counterelectrode. (C) Diagrams of the densities of state, $N(E)$, as functions of energy, of the F1-P-F2 system depicted in (A). The faint diagrams in the background refer to the state of the device when the switch is open.

The rise in the upspin subband chemical potential of P has an effect on F1: the chemical potential of F1 must rise so that the chemical potential of its upspin subband aligns with that of P. If this did not occur, there would be a backflow of spin-polarized electrons from P to F1. In more precise terms (1), there is a generalized thermodynamic force F_m associated with \tilde{M} that drives upspins back into F1. Because spin and charge are attached to the same carrier, the electron, this force also acts as an electrical impedance that appears as an interfacial resistance at the F1-P interface. Thus, a constant-current source encounters an extra, spin-coupled impedance, R_s , which is calculated below. This mechanism was called "spin-charge coupling" in the original derivation (3) and can also be pictured (5) as a "spin bottleneck": the buildup of spins impedes the continued flow of spins (and, therefore, of electrons) into the region.

When the axes of magnetization of F1 and F2 are parallel, the chemical potential of F2 rises so that its upspin subband chemical potential aligns with that of P ($E_{F,F2}$ in Fig. 1C). The effect is similar to the effect on F1. If the floating probe to F2 were to be short-circuited to ground, a current of upspins would be driven through F2 to ground. Because of the open-circuit condition on the probe at F2, no current can

flow, and the chemical potential of F2 must rise by eV_{F2} , where $V_{F2} = IR_s$, to prevent the current flow. Similarly, when the axes of magnetization of F1 and F2 are antiparallel, the chemical potential of F2 must drop so that its downspin chemical potential aligns with that of P. For orientations of \tilde{M}_1 and \tilde{M}_2 that vary between parallel and antiparallel, V_{F2} varies as $V_{F2} = IR_s \cos\theta$, where θ is the angle between \tilde{M}_1 and \tilde{M}_2 .

The change of chemical potential has been derived (3, 6) to be $eV_s = \eta_2 \tilde{M} / \chi$, where χ is the Pauli paramagnetic susceptibility of P. Some physical insight can be gained by noting that \tilde{M} / χ has the units of magnetic field and can be thought of as the effective magnetic field associated with the nonequilibrium spins. Therefore, $\beta \tilde{M} / \chi$ is the Zeeman energy of a spin-polarized electron in the presence of the field generated by all of the nonequilibrium spins (and is the source of the thermodynamic force F_m). Combining the above expressions for I_m , \tilde{M} , and V_s and using a free-electron expression for the susceptibility $\chi = \beta^2 N(E_F) = \beta^2 n / 2E_F$, where n is the density of conduction electrons, one finds (for the case $d \ll \delta$)

$$R_s = \frac{V_s}{I_e} = \frac{\eta_1 \eta_2}{e^2} \frac{T_2 E_F}{1.5 n A d} \quad (1)$$

Note that V_s is expected to be linear with I_e and should have units of impedance.

This device can be called a bipolar spin switch because the output voltage depends on the orientation of the electron spins. The voltage gain is bipolar, its magnitude depends on the relative orientation of the magnetizations \tilde{M}_i and can be quite large, and the device shows a memory effect associated with the coercivities of the magnetic films. Furthermore, although most measurements of prototype three-terminal devices (Fig. 1A) were made with high-impedance voltmeters, the terminal to F2 can be attached to ground through a low-impedance load, and the device operation would be analogous to a bipolar transistor; this device may be called a bipolar spin transistor. The terminal to F1 carries the emitter current, I_e ; that to P carries the base current, I_b ; that to F2 carries the collector current, I_c ; and the current gain is $G = I_c / I_b$.

To generalize this analogy, the Shockley-Haynes experiment (7) established the existence of two kinds of charge carriers (electrons and holes) in semiconductors by making a time-resolved transport measurement that used rectifying metallic point contacts to measure the chemical potential of the minority carriers (holes). The coexistence of two carrier populations over useful time and length scales and their mutual dynamics result in the device characteristics of the bipolar transistor (8). Similarly, after tunneling experiments (9) showed that fer-

romagnetic films could be used to spin polarize electric current, the spin injection experiment (3) demonstrated that the spin degree of freedom could be used to lift the degeneracy of carriers in metals and create two kinds of charge carriers (spin up and spin down). This experiment made use of parallel (antiparallel) ferromagnetic films for the measurement of the chemical potential of the majority (minority) carriers and proved that these two populations can coexist over useful time and length scales. It is their mutual dynamics that result in the characteristics of the spin transistor (10).

To measure the floating voltage V_{F2} , one must define a ground. A convenient choice is the nonmagnetic metal counterelectrode N (Fig. 1B), whose chemical potential is always aligned with the average chemical potential of P ($E_{F,P}$ in Fig. 1C). Note that it is not necessary to drive current into the vicinity of N. This geometry was chosen for its convenient symmetry and to demonstrate that N would function correctly in the presence of nonequilibrium spins. Although this geometry is vaguely similar to that of a Hall measurement, it is unique in that it utilizes F2 as a sensor of the chemical potential of the individual spin subbands of P.

Next, it is necessary to manipulate the orientations of \tilde{M}_1 and \tilde{M}_2 . Each film can be characterized by a coercivity $H_{c,i}$, and application of an external field H in the plane of the films will result in the magnetizations of F1 and F2 traversing similar hysteresis loops (Fig. 2A). When F1 and F2 are composed of the same material, the voltage V_{F2} is expected to be positive whenever the orientations \tilde{M}_i are aligned and negative when antialigned (Fig. 2B) (11). This effect was demonstrated in the original spin injection experiment (3), which was performed with a bulk metal. Because antiparallel orientation occurs only over the field range $H_{c,2}$ to $H_{c,1}$, it is necessary to maximize this difference through the fabrication of films with differing values for $H_{c,i}$. Designers can achieve this by using shape anisotropies, different materials for F1 and F2 (with intrinsically different coercivities), anisotropies associated with the substrate or with deposition conditions, or by coupling the magnetization of one of the films with that of a ferromagnetic or antiferromagnetic underlayer, which effectively "biases" its magnetization. In all samples used to collect the data below, F1 and F2 had a shape anisotropy, and one sample used a different material for each film.

An examination of the idealized hysteresis loops (Fig. 2A) provides an explanation of the memory effect mentioned above. If both films are aligned along $-\hat{H}$ (the bottom portion of the loop) and the field is increased along $+\hat{H}$ until one of the films has flipped its orientation ($H_{c,1} < H <$

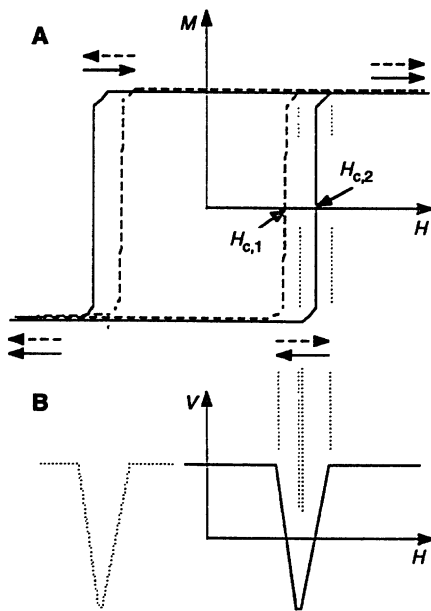


Fig. 2. Expected signal as a function of magnetization states of F1 and F2. (A) Hysteresis loops for F1 (dashed) and F2 (solid). Arrows represent parallel and antiparallel orientations of F1 and F2. $H_{c,i}$ coercivity of the two films. (B) Dependence of voltage on externally applied field. Solid line, sweeping up in field; dotted line, sweeping down [along the top portion of the loop in (A)].

$H_{c,2}$), then the decrease of H and return to $H = 0$ will result in a state in which F1 and F2 are antiparallel. Thus, there should be two stable magnetization states at $H = 0$ and two corresponding voltage states.

Prototype devices were fabricated on sapphire substrates. The ferromagnetic films of four samples were composed of permalloy with an approximate composition $\text{Ni}_{79}\text{Fe}_{21}$ and a thickness of 70 nm. A fifth sample used permalloy for F1 and Co for F2. A magnetization measurement of a permalloy test film showed a fairly square hysteresis loop with a coercivity of order 10 Oe and an in-plane anisotropy of about 10 Oe. A cobalt test film had a similar coercivity. I chose gold as the paramagnetic material so that I could also measure T_2 (12), for which no such measurement existed for gold. The device geometry (Fig. 1B) was defined with photolithography and liftoff, which etched windows in the insulating films of Al_2O_3 that separated the metallic layers. These windows had area $A = 10^{-2} \text{ mm}^2$. The voltage measurements were made with radio-frequency superconducting quantum interference device (SQUID) (13) amplifiers. Two SQUID voltmeters were used; I calibrated one by measuring the resistance of a gold wire. This calibration also verified the polarity of the voltage measurements. Although most measurements were made with dc current, ac measurements were also made, which confirmed the dc results.

An example of the data is shown in Fig. 3A. The signals were linear with current, and the signal magnitude is given in units of impedance (calculated with the total bias current). Currents of typically 0.1 to 10 mA were used, and voltages of order 10^{-8} V were recorded; the dynamic range of the SQUID voltmeters is 10^{-7} V , and this was

the only limit to the observed voltage magnitudes. The shape, width, and sign of the data conform to the expectations of a spin injection signal (Fig. 2B), and similar signals were recorded for sweeps of magnetic field along the \hat{x} and \hat{z} axes (sweeps in the plane of the films). Note that the signal is bipolar. The nonzero median is consistent with a slight asymmetry in the placement of the windows F2 and N (Fig. 1B). All samples showed nonzero offsets that ranged from 1 microhm to several milliohms but were typically a few tens of microhms. Because the coercivities of F1 and F2 are so close in value, the spin-coupled signal is observed only over a small range $H_{c,1} - H_{c,2} \approx 4 \text{ Oe}$. The observed signals must represent a lower limit of the actual value of R_s because it is impossible to know whether the films are completely antiparallel. Despite this possible source of error, the signals were quite reproducible, typically $\pm 25\%$, and consistent from sample to sample. The small hump at $H \approx -8 \text{ Oe}$ suggests that magnetic anisotropies exist that prevent the films from aligning completely when $H = \pm 50 \text{ Oe}$. When H approaches H_c , the magnetizations briefly come closer to alignment before one film flips its magnetization to an antiparallel alignment. The asymmetry of the dips relative to $H = 0$ confirms the existence of an in-plane anisotropy in this sample.

The memory effect is evident in the data (Fig. 3B). Initially, the external field was negative, and both M_1 and M_2 were oriented along $-\hat{H}$. An increasing field sweep is halted when the voltage begins to drop as a result of the realignment of one of the films in the vicinity of $H = +H_{c,1}$. Reversing the field sweep results in a low voltage until this film reorients at $H = -H_{c,1}$ and the origi-

nal voltage is recovered. Note the existence of two stable voltage states, associated with two stable magnetization states, at $H = 0$. The fact that these two states differ by less than the full voltage dip $2IR_s$ and that V_{F2} drifted to an intermediate value while the field sweep was halted (Fig. 3B, closed symbols) is probably because $H_{c,1}$ and $H_{c,2}$ are so close in value that F1 (or F2) had not completely flipped its orientation at the point where the external field sweep was reversed.

The spin-coupled impedance R_s (Eq. 1) is inversely proportional to the sample volume (for $d < \delta_s$). This is because \tilde{M} is a magnetization density, and the same number of polarized spins will give a larger \tilde{M} if the volume Ad is reduced. This scaling has been verified with measurements of prototypes that are identical except for the thickness d of the nonmagnetic layer. In a series of four samples for which F1 and F2 were permalloy, $R_s Ad$ was constant for the thickness range 0.1 to 1.5 μm and was exponentially diminished for a thickness much greater than the spin depth. The observed value of $R_s Ad$ in a fifth sample, which used Co for F2, was about five times larger than for the permalloy samples. A sixth sample, configured as a control with a nonmagnetic material for F1, showed no signal. The magnitudes of the spin-coupled signals for these prototype devices are quite high, much larger than impedances associated with the electrical resistivity of the Au. For the permalloy-Au-Co sample, for example, $2R_s = 0.8 \text{ milliohms}$, about four orders of magnitude larger than the resistive voltage drop across the thickness of the film. The signal magnitudes were constant over the

Fig. 3. Data from a prototype with $d = 98 \text{ nm}$. Under constant bias current, the voltage is recorded as the magnetic field is changed. (A) An example of data. Solid line, sweeping up in field; dotted line, sweeping down. (B) An example of a memory effect. There are two stable voltage states at $H = 0$. Lines are as in (A); solid symbols, change of voltage while field sweep is halted. (Inset) Expanded view of feature at $17 \pm 2 \text{ Oe}$ in (A). $I = 0.2 \text{ mA}$.

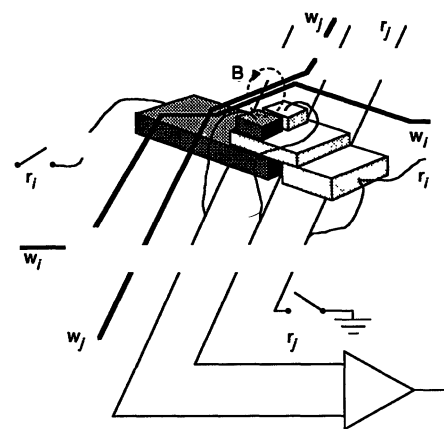
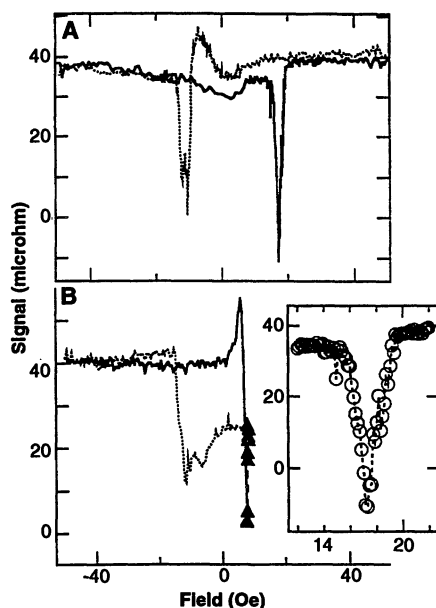


Fig. 4. A spin-switch storage element in an idealized nonvolatile solid-state memory array. Current pulses in heavy lines w_i and w_j produce local magnetic fields that write a magnetization orientation to F2. A current pulse sent through lines r_i and r_j results in a voltage pulse that is amplified and then read. In a real device, passive elements, such as diodes or resistors, would be incorporated to isolate each element.

experimentally convenient temperature range of 4 to 65 K and are not expected to diminish by more than a factor of 3 or 4 at room temperature (12).

Characteristics of the spin transistor are appropriate for numerous applications, such as an element in a solid-state non-volatile memory array (Fig. 4). Here F1 would be composed of a ferromagnet with a relatively large coercivity, and the film would be magnetically biased so that one edge of the hysteresis loop would be near $H = 0$. Film F2 would have a smaller coercivity. An initial, saturating magnetic field would align all of the films. An array of wires fabricated over the elements would write the state of the switch (14); the passage of current pulses through write wires w_i and w_j would provide a field pulse of one polarity or another adequate to orient F2 either parallel or antiparallel to F1. The operator could then read the state of the element by closing switches to lines r_i and r_j and sending a current pulse through the switch to ground. A voltage pulse of plus or minus polarity is sent to an amplifier at the end of read line r_j . Because the signal is bipolar, the discriminator can be set to zero, and the pulse is easily amplified. The result would be a solid-state nonvolatile memory, integrated on the same semiconductor chip as the logic elements and able to be accessed with comparable speed. A single element (Fig. 4) can be used as a magnetometer, like the sensing element of a read head for disks and tapes. This single element, in conjunction with a single write wire, also represents a five-terminal embodiment of the spin transistor used as a current, or power, amplifier in which a small, digitally modulated write current modulates a larger read current. The speed of the device is determined by carrier diffusion, spin relaxation, and domain switching times, with the latter imposing a limit of about 10 GHz.

More generalized attributes give reason for optimism about future development. In an analysis that parallels transistors, the spin transistor has a high degree of spin-polarized emission (≈ 1), a high fraction of spin transmission (≈ 0.96) and spin collection (≈ 1), and (on the basis of measurements of spin impedances) a gain of order 1000. The inverse scaling of signal with sample volume bodes well for microfabrication (15), although stable domain configurations (such as the "window pane") will be required as film dimensions are reduced. It has been shown that high-quality transition-metal ferromagnet films can be grown on silicon (16), so spin-transistor devices could readily be integrated with silicon technology. Spin injection in two-dimensional electron gases has not yet been attempted and offers other possibilities for

integrated devices (17). If spin injection in semiconductors can be demonstrated, the fourfold multiplicity of carriers would permit the creation of entirely new categories of devices.

REFERENCES AND NOTES

1. M. Johnson and R. H. Silsbee, *Phys. Rev. B* **35**, 4959 (1987); see appendix for the generalized solution.
2. A. G. Aronov, *Sov. Phys. JETP* **24**, L32 (1976) [translation from *Pis'ma Zh. Eksp. Teor. Fiz.* **24**, 37 (1976)].
3. M. Johnson and R. H. Silsbee, *Phys. Rev. Lett.* **55**, 1790 (1985); *Phys. Rev. B* **37**, 5312 (1988); *ibid.*, p. 5326.
4. The longitudinal relaxation time T_1 refers to a change of spin orientation along a direction parallel with an applied field and thus involves a change of energy. The transverse relaxation time T_2 refers to changes of spin orientation that are not accompanied by a change of energy. In the approximation of negligible external fields, we will assume that T_2 is the appropriate parameter.
5. M. Johnson, *Phys. Rev. Lett.* **67**, 3594 (1991).
6. R. H. Silsbee, *Bull. Magn. Resonance* **2**, 284 (1980).
7. J. R. Haynes and W. Shockley, *Phys. Rev.* **75**, 691 (1949).

8. J. Bardeen and W. H. Brattain, *ibid.*, p. 1208; and references therein.
9. R. Meservey, D. Paraskevopoulos, P. M. Tedrow, *Phys. Rev. Lett.* **37**, 858 (1976).
10. The nonlinear characteristic of *pn* junctions results in power gain in the transistor. The FN junctions have not shown nonlinearity, and power gain in the three-terminal embodiment of the spin transistor (for the case where N is Au) is thus unlikely.
11. When F1 and F2 are different materials, the sign convention of the expected effect in Fig. 2B may reverse if η_1 and η_2 have opposite signs.
12. M. Johnson, *Phys. Rev. Lett.*, in press.
13. Commercial SQUID from Biomagnetic Technologies, Inc.
14. A similar technique is used for the manipulation of the magnetization states of magnetoresistive films; see A. V. Pohm, J. S. T. Hwang, J. M. Daughton, D. R. Krahn, V. Mehra, *IEEE Trans. Magn.* **24**, 3117 (1988).
15. Surface states, which impair semiconductor device characteristics as devices are miniaturized, have no analog in spin devices.
16. G. A. Prinz, *Science* **250**, 1092 (1990); R. F. C. Farrow *et al.*, *Mater. Res. Soc. Symp. Proc.* **102**, 483 (1988).
17. S. Datta and B. Das, *Appl. Phys. Lett.* **56**, 665 (1990).
18. I acknowledge a useful conversation with E. Yablouovitch.

5 November 1992; accepted 25 January 1993

Structure of Langmuir-Blodgett Films of Disk-Shaped Molecules Determined by Atomic Force Microscopy

Jack Y. Josefowicz,* Nicholas C. Maliszewskij,
Stefan H. J. Idziak,† Paul A. Heiney,‡ John P. McCauley, Jr.,§
Amos B. Smith III

Monolayer Langmuir-Blodgett films of a discotic mesogen have been studied with atomic force microscopy (AFM). These measurements confirm the "edge on" arrangement for the disk-shaped molecules suggested by surface pressure-area isotherms and show that the molecules form columns that are separated by 17.7 angstroms \pm 10 percent. Column alignment is found to be predominantly along the film deposition direction, with an angular spread of 35°. The AFM images also show that the mean disk separation within the columns is 5.1 \pm 1.3 angstroms, in good agreement with x-ray diffraction (XRD) results. Room-temperature XRD measurements on bulk samples of the same material indicate a disordered-hexagonal liquid crystalline mesophase, with a column-to-column spacing of 19.9 \pm 0.2 angstroms.

Thin films that display anisotropic dc conductivity are of interest both because they are model low-dimensional systems and because of their potential applications. Anisotropy within the plane of the film may be valuable for display applications, whereas films that are highly conductive in the direction normal to the surface could be used as pressure sensors and similar devices (1). A promising approach to the preparation of such films is the formation of conductive Langmuir-Blodgett (LB) (2) films. Typically, LB films are composed of organic, amphiphilic linear chains. However, disk-shaped molecules exhibiting columnar liquid crystalline mesophases (3), which

generally have rigid, π -conjugated cores and flexible hydrocarbon substituents, although not manifestly amphiphilic, have under some circumstances been shown to form Langmuir (4-8) and LB (4, 8) films. Furthermore, the conductivity of a number of discogenic compounds has also been observed to increase by up to six orders of magnitude after doping by electron acceptors such as iodine (9). This conductivity can be highly anisotropic, with most of the conduction occurring along the column axis.

Surface spreading pressure isotherm measurements (2) suggest that, depending on their architecture, discogenic mesogens typically exhibit one of two possible orien-